Hindawi
Adsorption Science & Technology
Volume 2022, Article ID 1668924, 19 pages
https://doi.org/10.1155/2022/1668924

Research Article

Finite Element Method-Based Spherical Indentation Analysis of Jute/Sisal/Banana-Polypropylene Fiber-Reinforced Composites

Nitish Kaushik,[1] Ch. Sandeep,[2] P. Jayaraman,[3] J. Justin Maria Hillary,[4] V. P. Srinivasan,[5] and M. Abisha Meji[6]

[1]*Department of Production and Industrial Engineering, Birla Institute of Technology, Mesra, 835215, Ranchi, Jharkhand, India*
[2]*Department of Mechanical Engineering, Institute of Aeronautical Engineering, 500043, Hyderabad, Telangana, India*
[3]*Department of Mechanical Engineering, Prathyusha Engineering College, 602025, Thiruvallur, Tamil Nadu, India*
[4]*Department of Mechatronics Engineering, Sri Krishna College of Engineering and Technology, 641008, Coimbatore, Tamil Nadu, India*
[5]*Department of Mechanical Engineering, Sri Krishna College of Engineering and Technology, 641008, Coimbatore, Tamil Nadu, India*
[6]*Department of Physics, School of Engineering and Applied Sciences, Kampala International University, Western Campus, Uganda*

Correspondence should be addressed to M. Abisha Meji; abisha.meji@kiu.ac.ug

Received 26 July 2022; Revised 29 August 2022; Accepted 5 September 2022; Published 20 September 2022

Academic Editor: Debabrata Barik

Material hardness of natural fiber composites depends upon the orientation of fibers, ratio of fiber to matrix, and their mechanical and physical properties. Experimentally finding the material hardness of composites is an involved task. The present work attempts to explore the deformation mechanism of natural fiber composites subjected to post-yield indentation by a spherical indenter through a two-dimensional finite element analysis. In the present work, jute-polypropylene, sisal-polypropylene, and banana-polypropylene composites are considered. The analysis is attempted by varying the properties of Young's modulus of fiber and matrix, diameter of fiber, and horizontal and vertical center distance between the fibers. The analyses results showed that as the distance between the fiber's center increases, the bearing load capacity of all composite increases nonlinearly. The jute fiber composite shows predominate load-carrying capacity compared to other composites at all L/D ratios and interference ratios. The influence of subsurface stress in lateral direction is minimal and gets reduced as the distance between the fiber centers increases. The variation in diameter of fiber influences significantly, i.e., beyond the L/D ratio of 1.0; for the same contact load ratio, the bearing area support is double for jute-polypropylene composite compared to sisal-polypropylene composite. Compared to the sisal-polypropylene composite, for the same interference ratio, the load-carrying capacity is two times high for banana-polypropylene composite, whereas four times high for jute-polypropylene composite, but this effect decreases as the L/D ratio decreases. In all the composites, the subsurface stress gets distributed as the L/D ratio increases. The ratio of fibers center distance to diameter of fiber influences marginally on the contact load and contact area and significantly on the contact stress for all the fiber-reinforced composites.

1. Introduction

Natural fibers are extensively used in the preparation of composites due to their low cost, low density, and biodegradable. The properties of natural fiber composite depend on source of fiber, fiber extraction, fiber preparation, fiber property, matrix preparation, matrix property, and fabrication process like hand molding, compression molding, injection molding, continuous pultrusion, and extrusion molding and their process parameters. Verma et al. [1] fabricated the alkali-treated sisal reinforced with starch and epoxy matrix biocomposites and investigated their mechanical and microstructure characteristics. The results revealed that epoxy-coated fiber composite showed improved property. Verma et al. [2] fabricated and

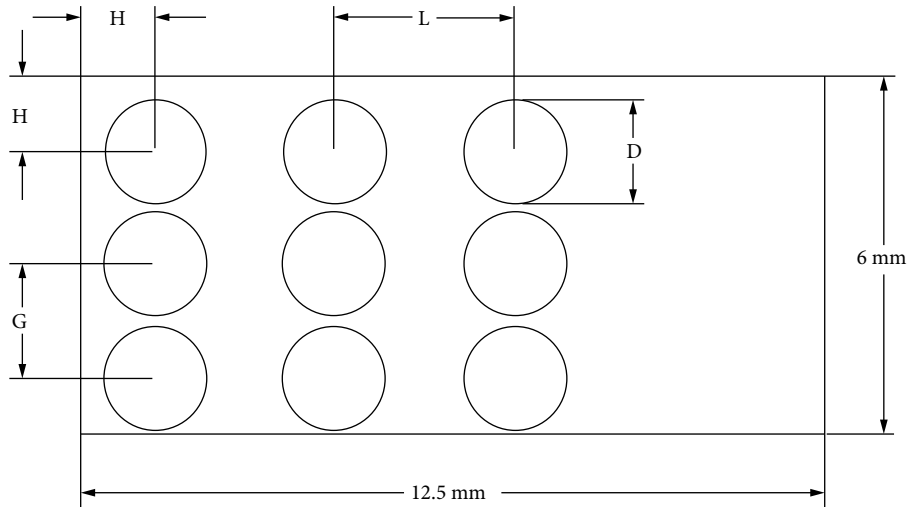

Figure 1: Geometrical modeling parameter.

experimentally characterized the jute and starch hybrid biocomposites. They concluded that water absorption significantly affected the mechanical properties of the composites. Verma et al. [3] investigated the mechanical and physical behavior of soy protein and sisal fiber-reinforced green composites. Vijay et al. [4] experimentally studied the raw and alkali-treated tridax procumbens fiber composites. The alkali-treated fiber-based composites showed improved thermal stability, tensile, and crystallinity. Dinesh et al. [5] investigated the influence of wood dust as fillers in the mechanical and thermal properties of jute –epoxy fiber composites. The results showed that padauk wood dust embedded composite improved the mechanical property, whereas rosewood dust enhanced the thermal stability of the composite. Jothibabu et al. [6] attempted to evaluate the hybridization effect on mechanical property through the different stacking sequence of areca sheath fiber/jute fiber/glass fabric fiber composites. Vijay et al. [7] examined the thermo-mechanical characteristics of Azadirachta indica seed powder and Camellia sinensis powder filled jute epoxy composites. Vijay et al. [8] studied the physical, chemical, thermal, mechanical, and morphological characteristics of treated and untreated Leucas aspera fibers. Vijay et al. [9] examined the physical and chemical properties of Vachellia farnesiana fibers. Sathish Kumar and Nivedhitha [10] studied the different weight fraction-based chemically modified kenaf fiber-epoxy composites. The results showed that 6% NaOH treated 40% weight fraction fiber composite showed improved mechanical property compared to others. The above natural fiber composites are fabricated with different orientation of fibers and ratio of fiber to matrix so finding their mechanical properties is an involved task. If a model or method is developed to find the mechanical properties in advance that may reduce cost and time incurred to fabricate the materials with required properties. Generally, the hardness values for the metallic materials are well known and are available in ASTM standard format, but the hardness values for natural fiber composites are unknown in most of the circumferences. Indentation-based hardness has direction benefits in different engineering applications like load-bearing mechanical elements and contact effects at different length scales in micro, meso, and macro applications. The pioneered indentation of metals was approached by Tabor [11]. The followers attempted in numerical, semianalytical, and analytical methods using different shapes of indenters indenting infinite half space to explore the plasticity role. Ishlinsky [12] attempted indentation of rigid perfectly plastic half space against a rigid sphere using the slip-line theory of plasticity and concluded that indentation hardness is three times of material yield strength, whereas Hill et al. [13] used flow theory for the same. Johnson [14] stated that indentation behavior of elastic perfectly materials against rigid indenter can be explored in deformation order of elastic, elastoplastic, and fully plastic deformations. Samuels and Mulhearn [15] explored the deformation behavior of half space against a blunt indenter and observed that subsurface deformation is in radial direction under the contact zone. The pioneer finite element method-based study was attempted by Hardy et al. [16], who detected that contact pressure changes from elliptical to rectangular and also observed that contact stress in axis symmetry is constant as the applied load increases. Follansbee et al. [17] compared their elastic-plastic indentation numerical results with the Hertz elastic solution and shallow and deep indentations experimental results and found good agreement with them. Giannakopoulos et al. [18] found constitutive relations for applied normal load and indentation interference using finite element method for elastic and elastic-plastic material against a Vickers indenter. Komvopoulos and Ye [19] observed the behavior rigid sphere indentation against an elastic perfectly plastic half-space through the finite element study. The developed constitutive equations showed good agreement with Johnson [14] and concluded that material hardness is three times the yield strength of indented material. Park and Pharr [20] explored the elastic and plastic dominant regimes in elastic-plastic indentation. Mesarovic et al. [21] detected a decreasing trend in mean contact pressure for larger indentation which leads to the failure. Bhattacharya et al. [22] studied the elastic and plastic behavior with finite element approach at submicrometer scale and compared with experimental results. They said that continuum-

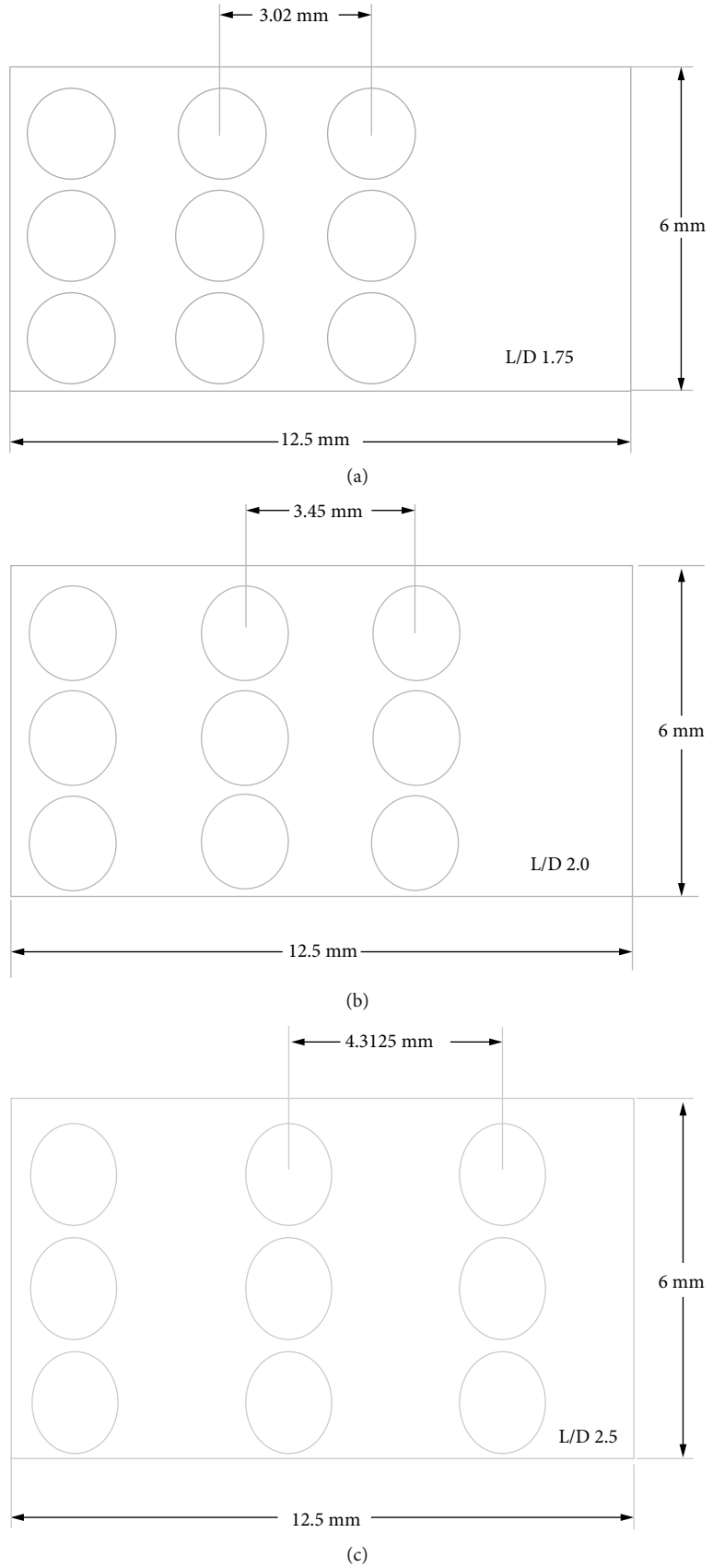

Figure 2: Continued.

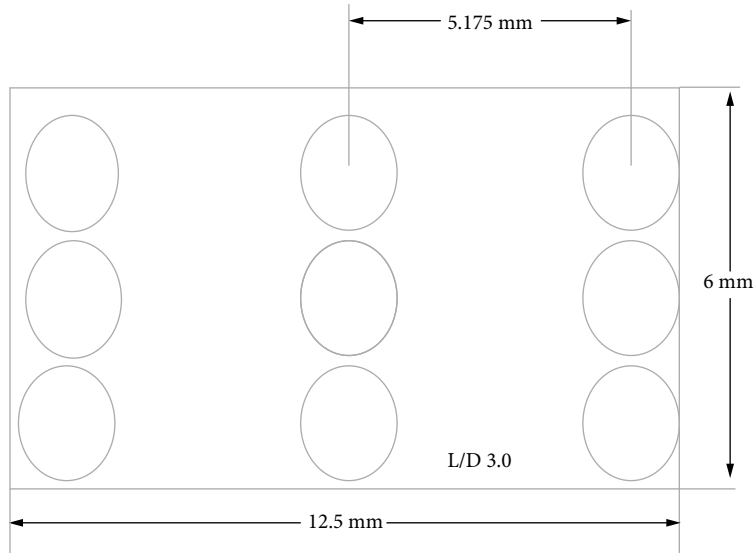

(d)

Figure 2: Models with different L/D ratios (by varying the distance between fiber centers).

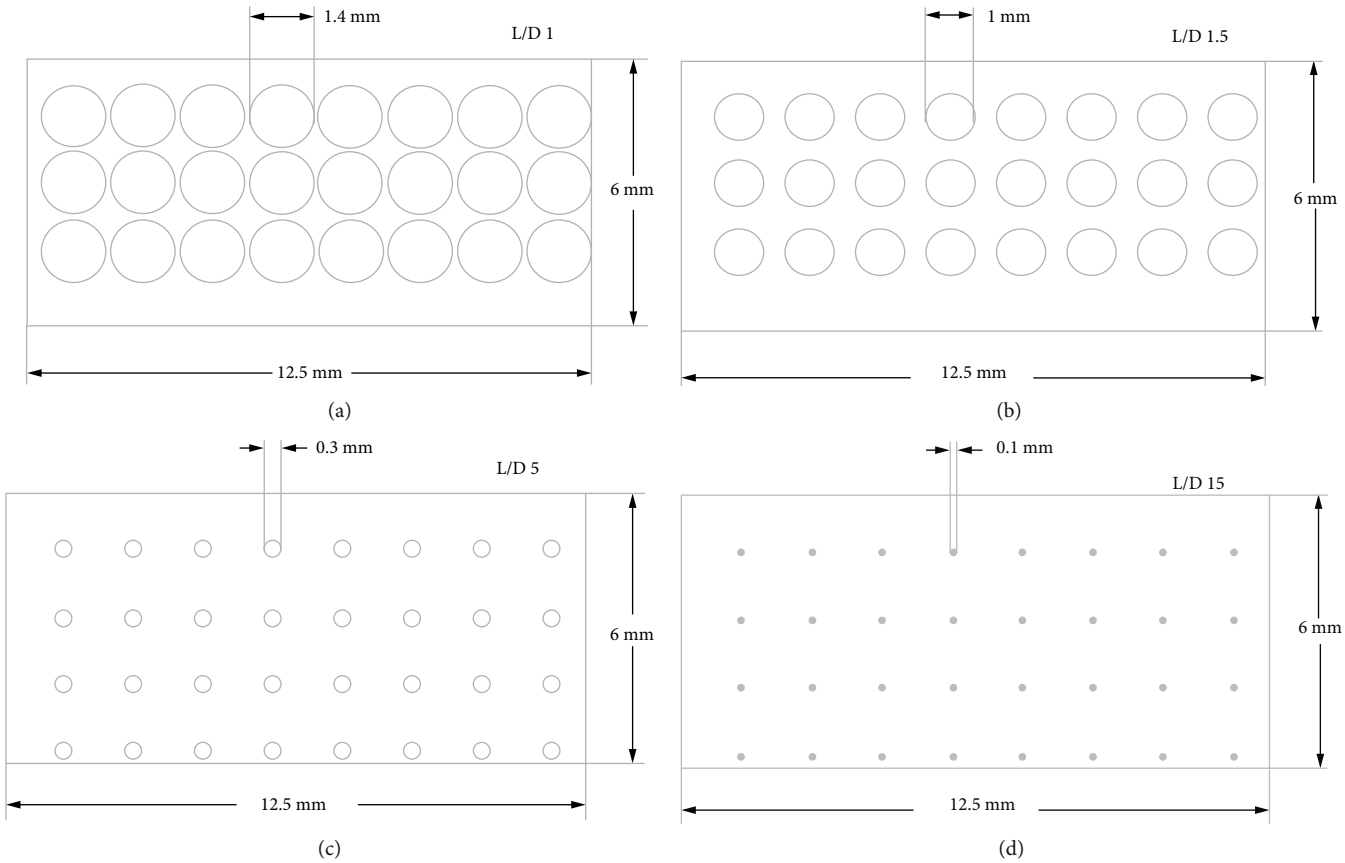

Figure 3: Models with different L/D ratios (by changing the fiber diameter).

based finite element approach can relate load and indentation at submicrometer scale in a well manner, and Knapp et al. [23] developed finite element approach-based nanoindentation method to expose the elastic modulus and hardness of layered medium.

Apart from the indentation models, flattening models are also approach by different researchers. Kogut et al. [24] analyzed deformation of a sphere asperity against a rigid flat through finite element approach and deduced empirical relations for contact parameters with

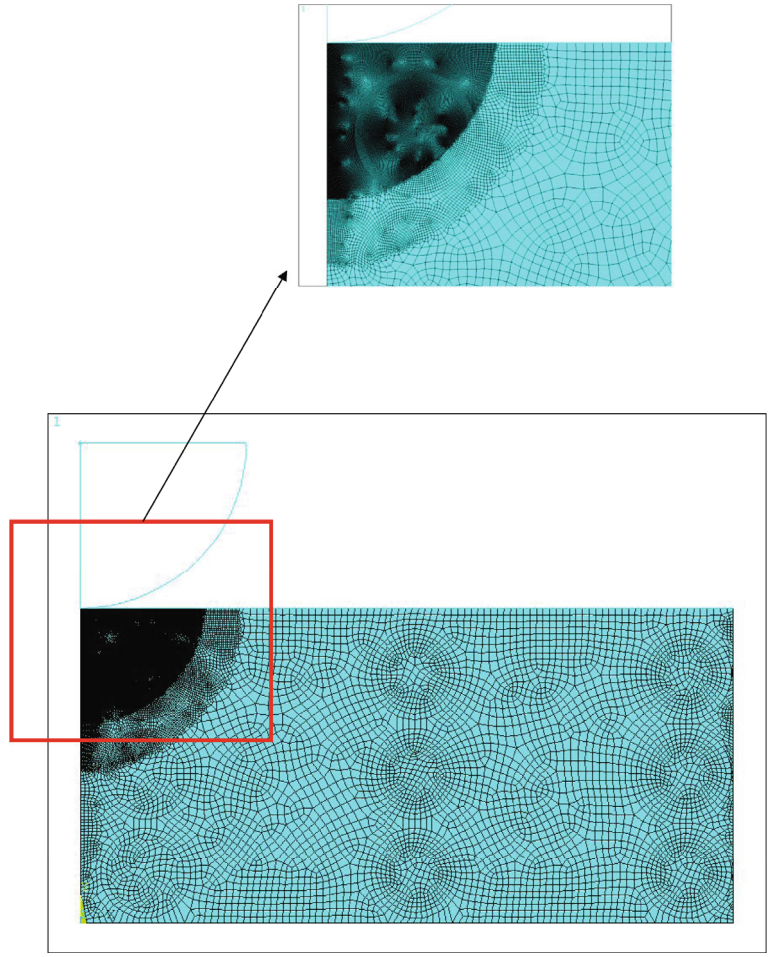

Figure 4: Meshed model of L/D 3.0.

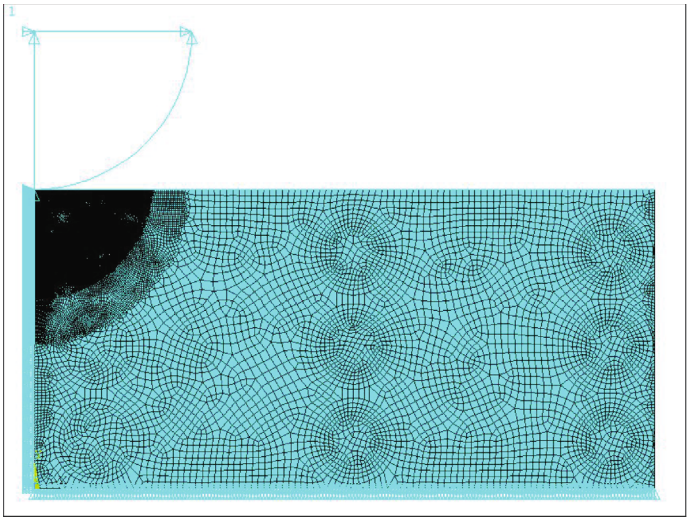

Figure 5: Finite element model of L/D 3.0 with boundary conditions.

interference as variable. Chang et al. [25] called as CEB model assumed volume conservation at the tip of spherical asperity and offered a simplified analytical contact area and contact load solution for the elastic-plastic contact deformation behavior similarly Thornton et al. [26] who provided a simplified analytical solution based on elastic perfectly plastic collision of spheres with truncated Hertz contact pressure distribution.

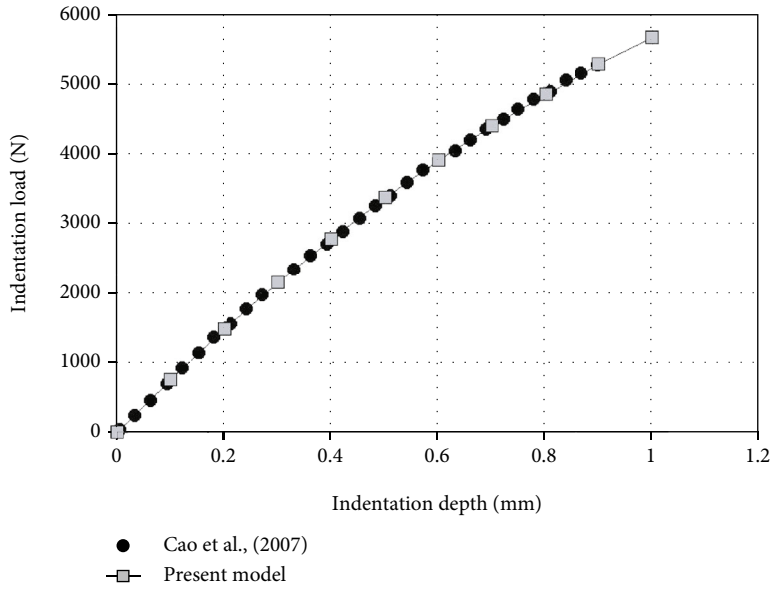

Figure 6: Validation of present model with Yanping Cao et al. [38] model.

Table 1: Physio-mechanical properties of fibers and matrix.

Fiber/matrix	Density (g/cm^3)	Tensile strength-Y (MPa)	Tensile modulus-E (MPa)	Poisson's ratio	Reference
Banana	1.35	600	17.85	0.30	[39]
Sisal	1.45	567	10.4	0.32	[39]
Jute	1.3-1.45	393-800	13-26.5	0.31	[40]
Polypropylene	0.9	27	0.8	0.41	[41]

Kocharski et al. [27] and Vu-Quoc et al. [28] provided more accurate finite element solutions with realistic elastic plastic deformation of spherical asperity during its loading, but they did not provide common solution for the global contact parameters. Kogut et al. [29] carried out a finite element-based loading and unloading of rigid sphere indentation in a half space for elastic-plastic materials. Meanwhile, Quicksall et al. [30] explored the effect of Young's modulus and yield strength properties impact on single asperity flattening model. Jackson et al. [31] extended the Kogut et al. [24] model for low to high E/Y values and developed empirical expressions for contact parameters with the variation of H/Y against the deforming contact geometry.

Brizmer et al. [32] explored the contact condition effects with the study of ductile and brittle materials with their respective failure criterions. Ovcharenko et al. [33] experimented with copper, stainless steel spheres, and sapphire flat and observed good agreement with the existing contact models. Jackson et al. [34] compared their results with the spherical indentation models of Komvopoulos et al. [19] and Kogut and Komvopoulos et al. [35]. Recently, Wagh et al. [36] analyzed the composite laminates with finite thickness using spherical indenter. Lei Zhou et al. [37] explored the influence of eccentricity and indentation modulus for an anisotropic elastic half space indented by a spherical rigid indenter.

The above-mentioned literature explored the different metallic materials' elastic-plastic indentation and flattening behavior, but the natural fiber composite materials indentation behavior is not explored in detail. The objective of the present work is to explore the indentation characteristics of elastic–plastic behavior of natural fiber composite materials for mostly using fibers and matrixes, and the present work attempted to develop an empirical relation to calculate material hardness of natural fiber composites when subjected to post-yield indentation through finite element analysis, by accounting the properties of matrix and fibers such as diameter of fiber, horizontal and vertical center distance between the fibers, and Young's modulus of fiber and matrix.

2. Modeling and Analysis Details

Mostly hardness of composite materials is found using ASTM D785 standard. In order to explain the effect of fiber and matrix properties, two-dimensional model is considered here, and the geometrical and modeling content are discussed in the below section.

2.1. Modeling Details. For the two-dimensional indentation analysis, a model having 12.5×6 mm and a spherical indenter of 3.175 mm radius as per the ASTM D785 standard are considered. The geometrical parameters for modeling are shown in Figure 1. The horizontal and vertical distance from the top of the specimen is (H), the horizontal distance between fiber centers is (L), the vertical

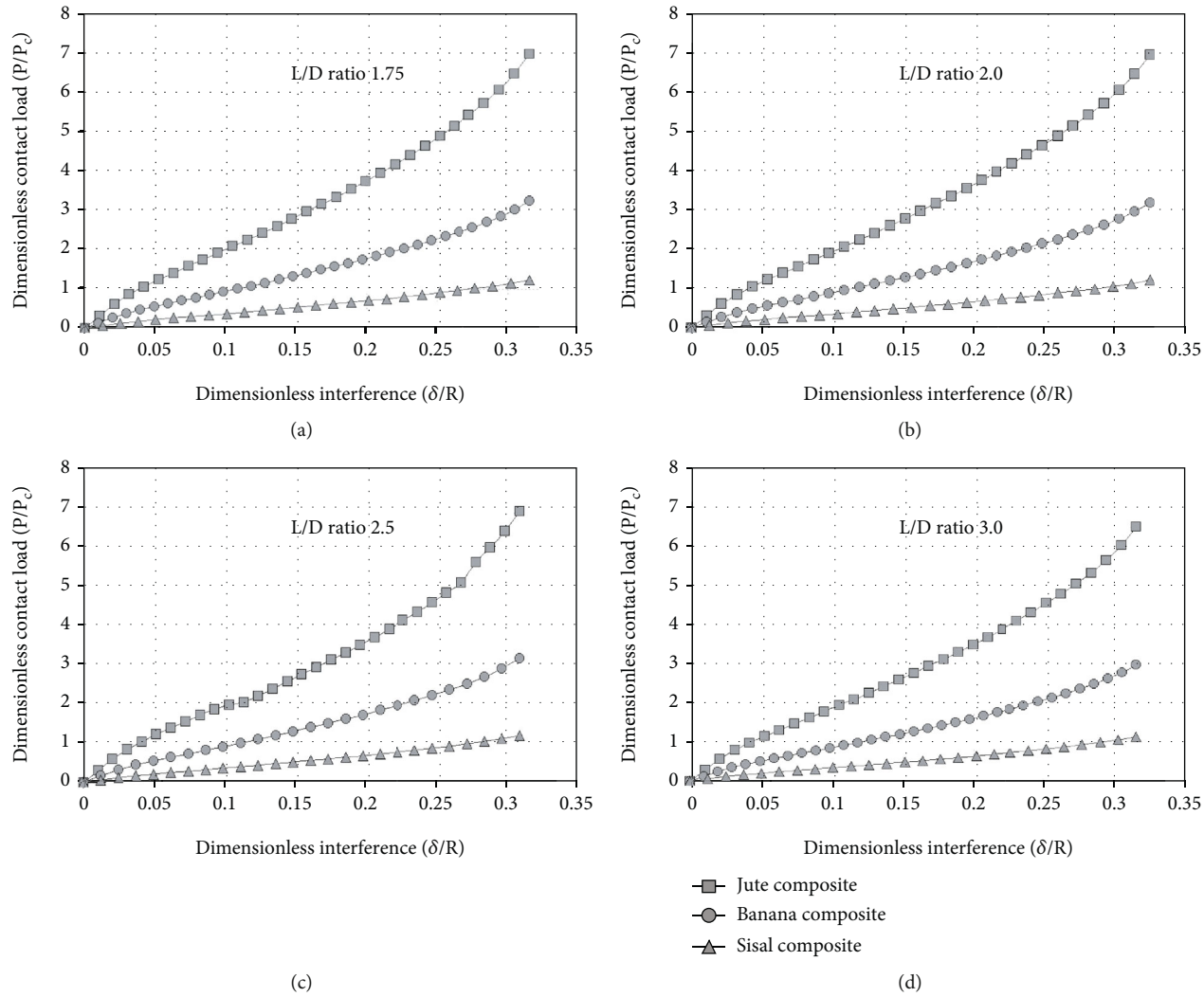

Figure 7: Contact load ratio for various *L*/*D* ratios.

distance between fiber centers is (G) and the diameter of the fiber is (D).

The distance between the fiber's center and the fiber diameter are most geometrically affecting parameters of the material hardness apart from the orientation of the fibers, so the distance between the fiber's center and the fiber diameter is taken as varying parameters of the present work. The different *L*/*D* ratios such as 1.75, 2.0, 2.5, and 3.0 are obtained by changing the distance between fibers center (http://i.e.by changing the horizontal length between fiber centers only), and the resultant models for different *L*/*D* ratios by changing the fiber diameter are given below in Figures 2(a)–2(d) and 3(a)–3(d), respectively.

2.2. Analysis Details. The finite element approach based ANSYS® package is employed in indentation analysis of natural fiber-reinforced composites. In order to mesh the above models, 8-noded 2D element (PLANE 183) is taken. The meshed model of *L*/*D* 3.0 is shown in Figure 4. It consists of 73,698 elements in which more than 60% of elements are occupied in the expected contact zone. A rigid spherical indenter is placed on the model. The surface contact pair between the rigid indenter and the model is established with frictionless condition. The top surface of the model consists of contact element (CONTA172), and the rigid indenter holds non-flexible elements (TARGE169). The nodes on the planar symmetry of the meshed model are constrained in horizontal direction, and the nodes on the bottom of the meshed model are constrained in all directions. The resultant finite element model having *L*/*D* 3.0 is shown in Figure 5. Similarly, all other models having different *L*/*D* ratios are modeled and meshed. The indentation is done by applying the displacement incrementally to the indenter with incremental substeps of maximum 8,000, and then, the contact parameters are extracted from each analysis results.

2.3. Validation of Present Model. The present finite element model is validated with Yanping Cao et al. [38] model, and the result shows a variation less than 1%. The indentation depth is given up to 1 mm in the present model. Figure 6 shows the indentation load versus indentation depth for the present model which shows the same behavior as Yanping Cao et al. [38] model.

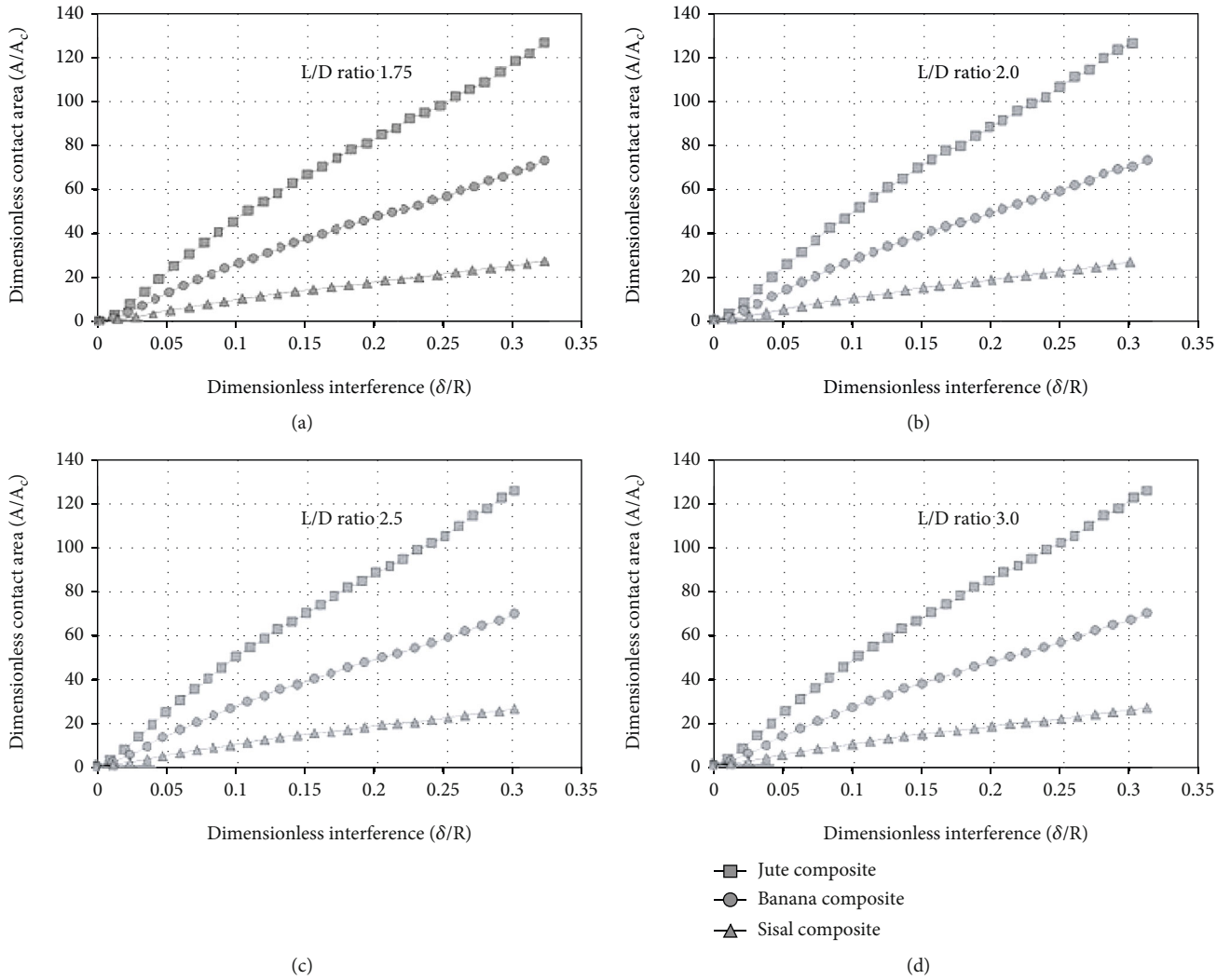

Figure 8: Variation of contact area ratio for various L/D ratios.

3. Results and Discussion

For the present indentation analysis, the most commonly using natural fibers and matrix are utilized which is given in Table 1 where the natural fiber-reinforced composite's E/Y ratio varies in the range of 18 to 40. The contact parameters are observed for every small step of the indentation to enumerate the influence of distance between fiber centers and fiber diameter.

3.1. Influence of Distance between Fiber Centers on Contact Parameters. The contact loads for every step are extracted from the analysis results.

3.1.1. Influence of Contact Load. The response of contact load ratio against interference ratio for the L/D ratios of 1.75, 2.0, 2.5, and 3.0 is shown in Figures 7(a)–7(d).

In Figure 7, as the dimensionless interference increases, the load-bearing capacity increases for all the fiber composites nonlinearly, but the trend looks similarly. The deviation among the load-carrying capacity increases as the interference ratio increases. For the same interference ratio, the jute fiber-based composite shows very high load-bearing capacity compared to all other composites. The sisal fiber-based composite shows very less load-carrying capacity, whereas the banana fiber-based composite behavior is intermediate so, for the increasing E/Y ratio, load-carrying capacity also increases. At the same interference ratio, as the L/D ratio increases, the load-bearing capacity increases marginally which is less than 3% for all composites.

3.1.2. Effect of Contact Area. The contact areas for every step are extracted from the analysis results. The contact area ratio against the interference ratio for the L/D ratios of 1.75, 2.0, 2.5, and 3.0 is shown in Figures 8(a)–8(d).

From the Figure 8, as the dimensionless interference increases, the contact area ratio increases for all the fiber composites, and the deviation among them also increases. Compared to sisal fiber composite, the jute fiber composite shows five times high bearing area ratio, whereas the banana fiber-based composite shows two times high bearing area ratio. In each composite, for the same interference ratio, as the L/D ratio increases, the contact area ratio marginally increases as like contact load ratio.

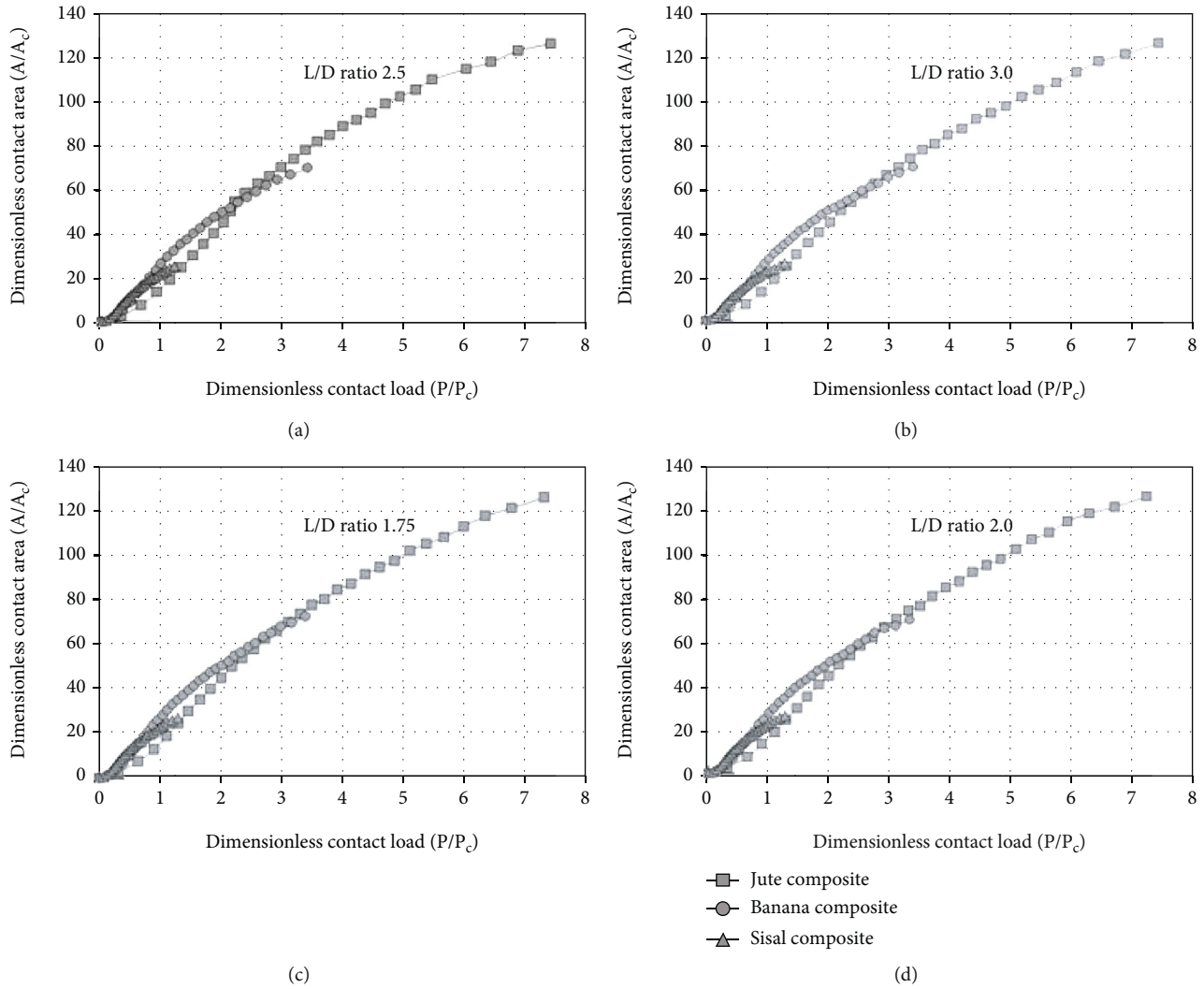

Figure 9: Response of contact area ratio vs contact load ratio for various L/D ratios.

3.1.3. Effect of E/Y Ratio on Contact Load and Area. Figures 9(a) and 9(b) shown below show the response of contact area ratio against contact load ratio for various L/D ratios. As contact load ratio increases, the contact area ratio also increases. For the same indentation depth, the jute fiber-reinforced composites have very high dimensionless contact area when compared to banana and sisal fiber-reinforced composites.

3.1.4. Effect of L/D Ratio on Contact Load and Area. Figure 10 shows the influence of L/D ratios on the contact area ratio with contact load ratio.

The influence of L/D ratios on all the composites is similar, but for the same contact load ratio, the bearing area is large for banana composite, and it is less for the jute composite and intermediate for sisal composite.

3.1.5. Effect of E/Y Ratio and L/D Ratio on Von Mises Stress Distribution. The three modes of deformation of polypropylene such as elastic, elastic-plastic, and plastic deformations are extracted from the analysis results. The Von Mises stress plots of the three mode of deformation are shown in Figures 11(a)–11(c). The Von Mises stress distribution is used to identify the areas in which the equivalent stress is maximum and minimum and its distribution pattern and also it is used to predict failure of the material.

The resultant Von Mises stress plots for jute-polypropylene composite at δ/R of 0.31496 for different L/D ratios are shown in Figures 12(a)–12(d). The influence of distance between the fiber centers on stress distribution is less.

Figures 13(a)–13(d) show the stress distribution in the banana-polypropylene composites of increasing L/D ratio at δ/R of 0.31496.The influence of increase in L/D ratio on stress distribution is marginal.

When compared to jute and banana fiber-reinforced composites, the stress distribution in sisal-polypropylene composite is significant. The resultant Von Mises stress plots for sisal-polypropylene composite at δ/R of 0.31496 for different L/D ratios are shown in Figures 14(a)–14(d).

3.2. Influence of Fiber Diameter on Contact Parameters. The contact loads for every step are extracted from the analysis results by accounting the influence of fiber diameter.

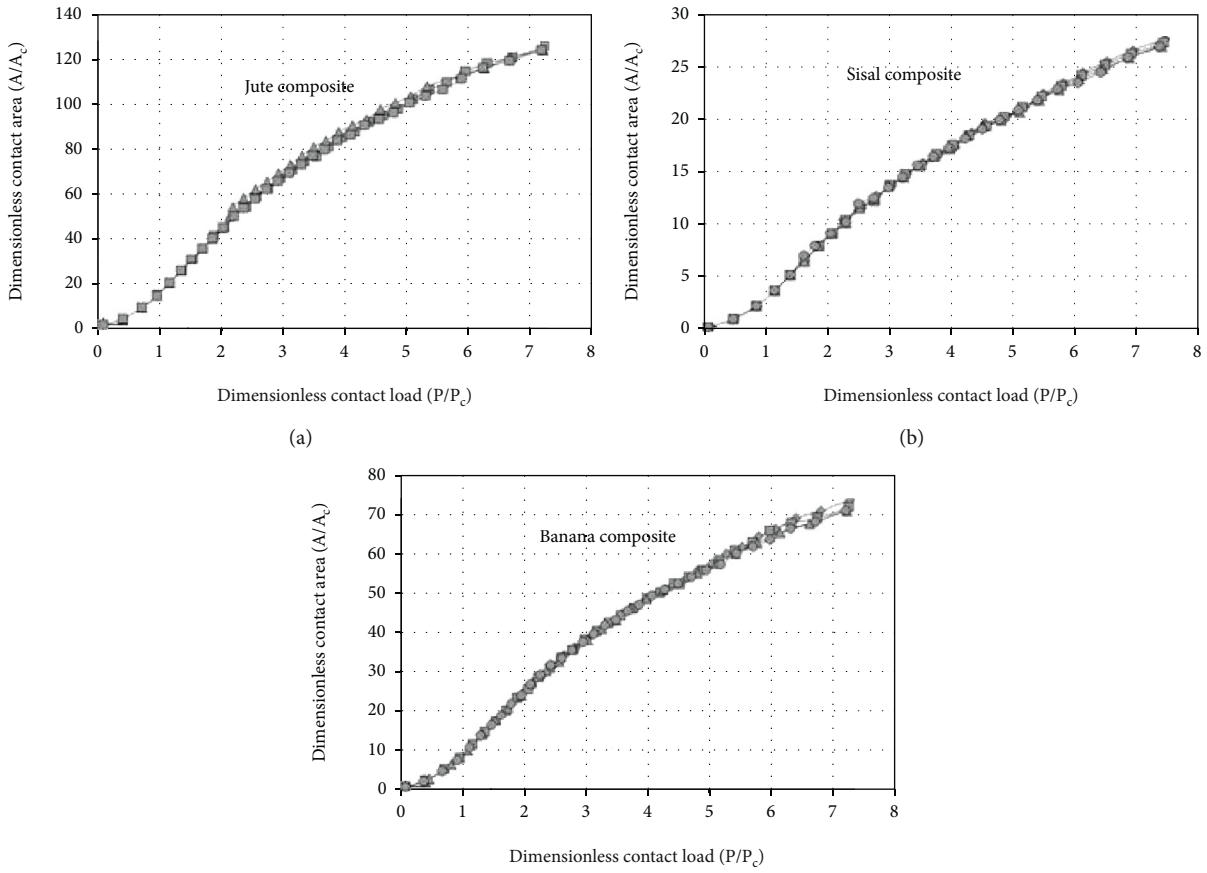

Figure 10: Response of contact area ratio vs contact load ratio for different composite.

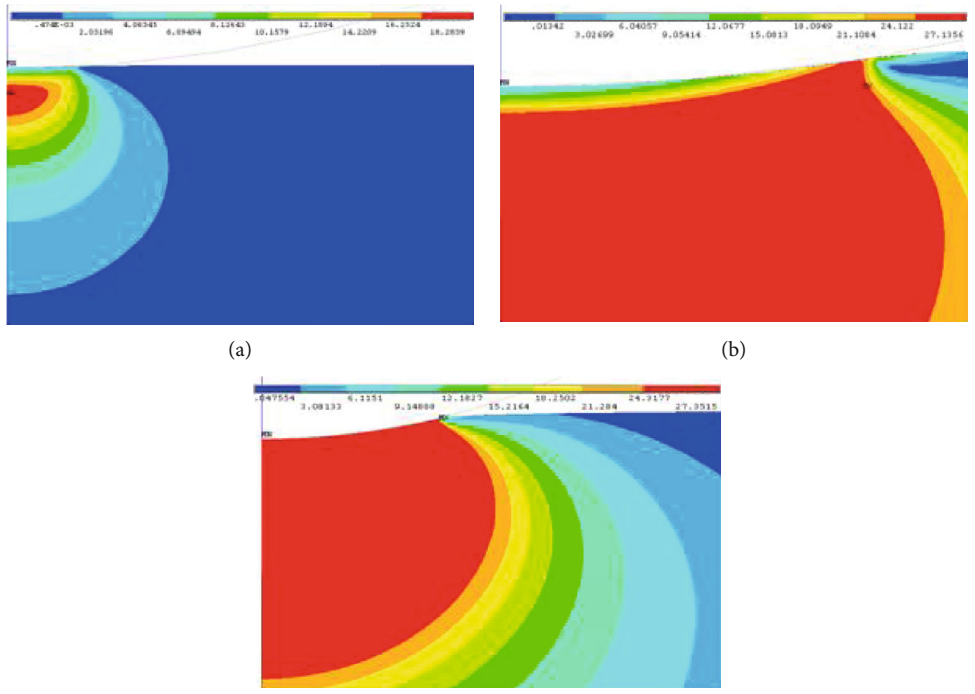

Figure 11: Von Mises stress plot for three modes of deformation of polypropylene matrix.

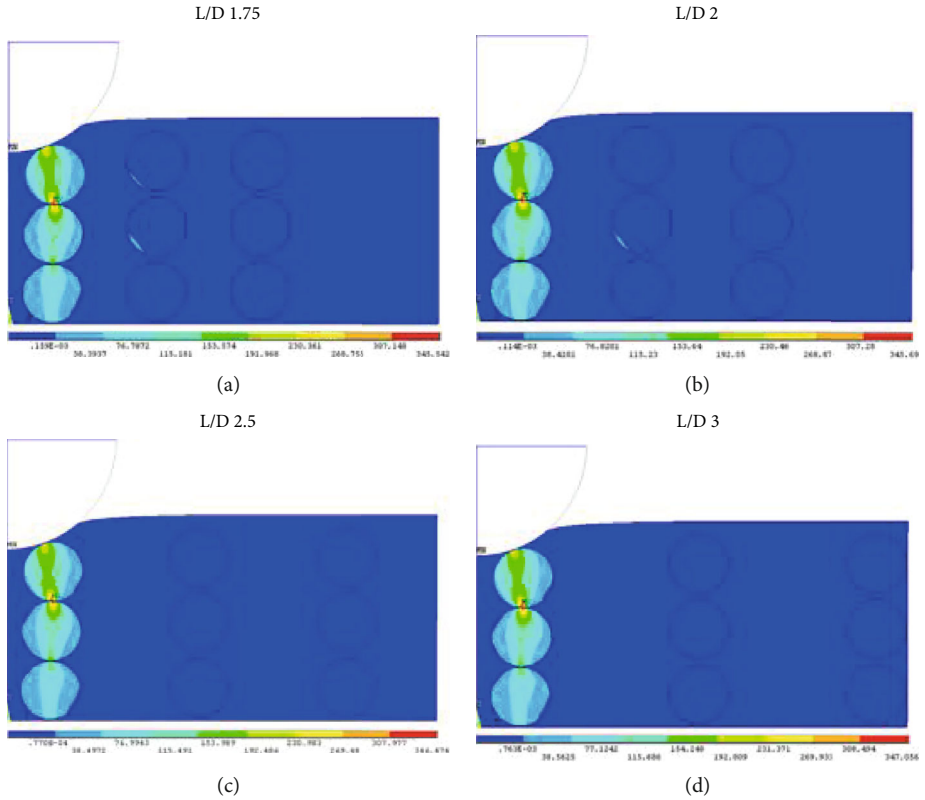

Figure 12: Von Mises stress plot for jute-polypropylene composite for various L/D ratios.

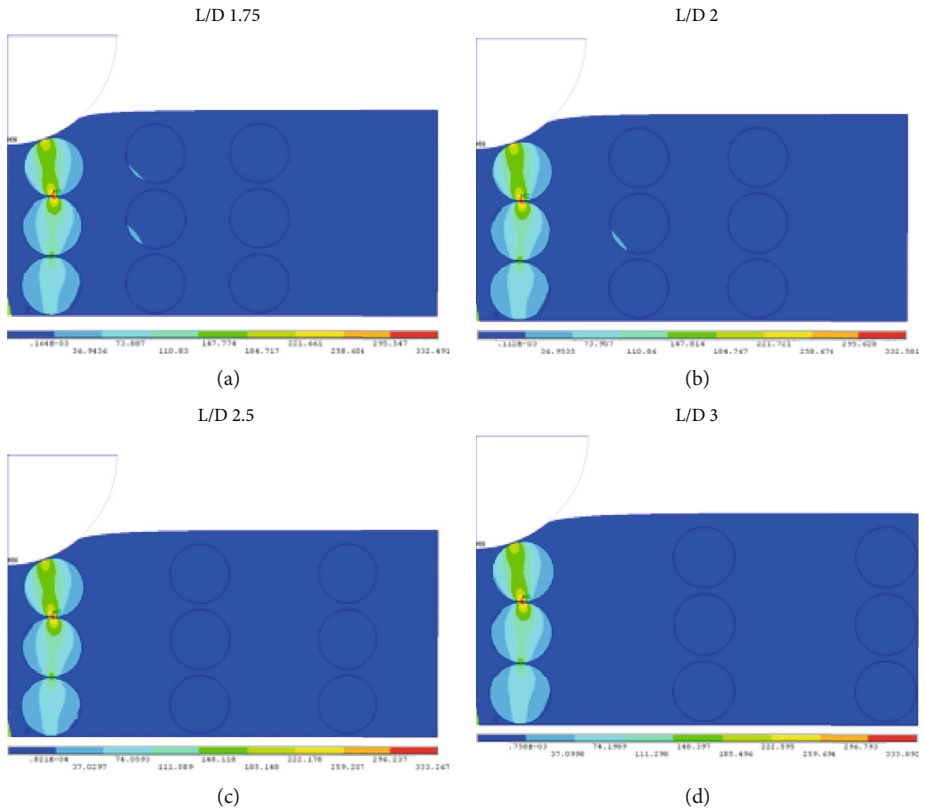

Figure 13: Von Mises stress plot for banana-polypropylene composite for various L/D ratios.

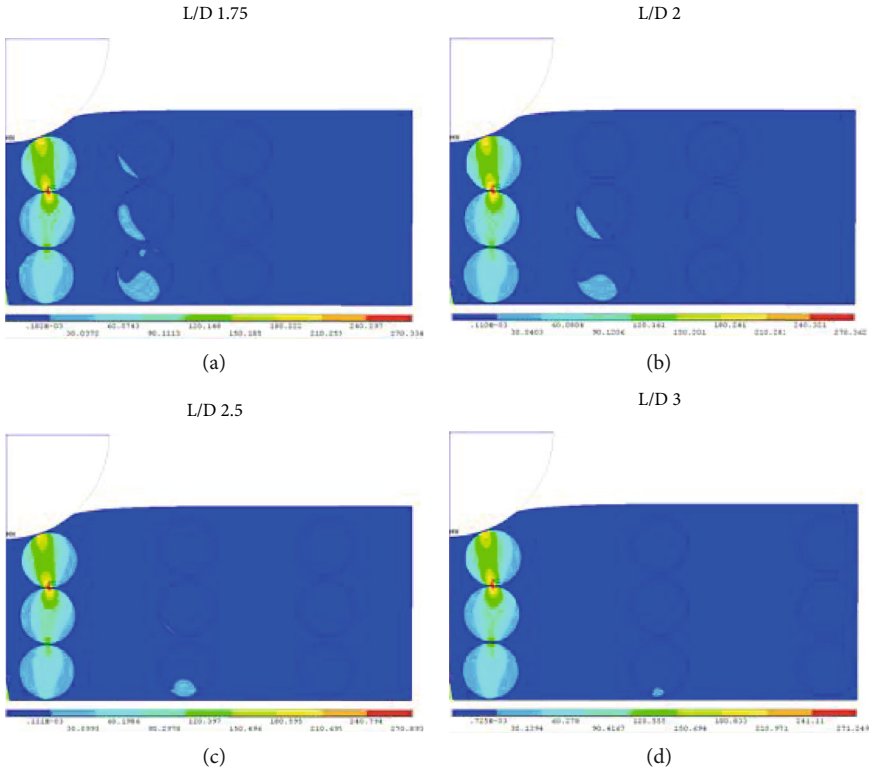

Figure 14: Von Mises stress plot for sisal-polypropylene composite for various L/D ratios.

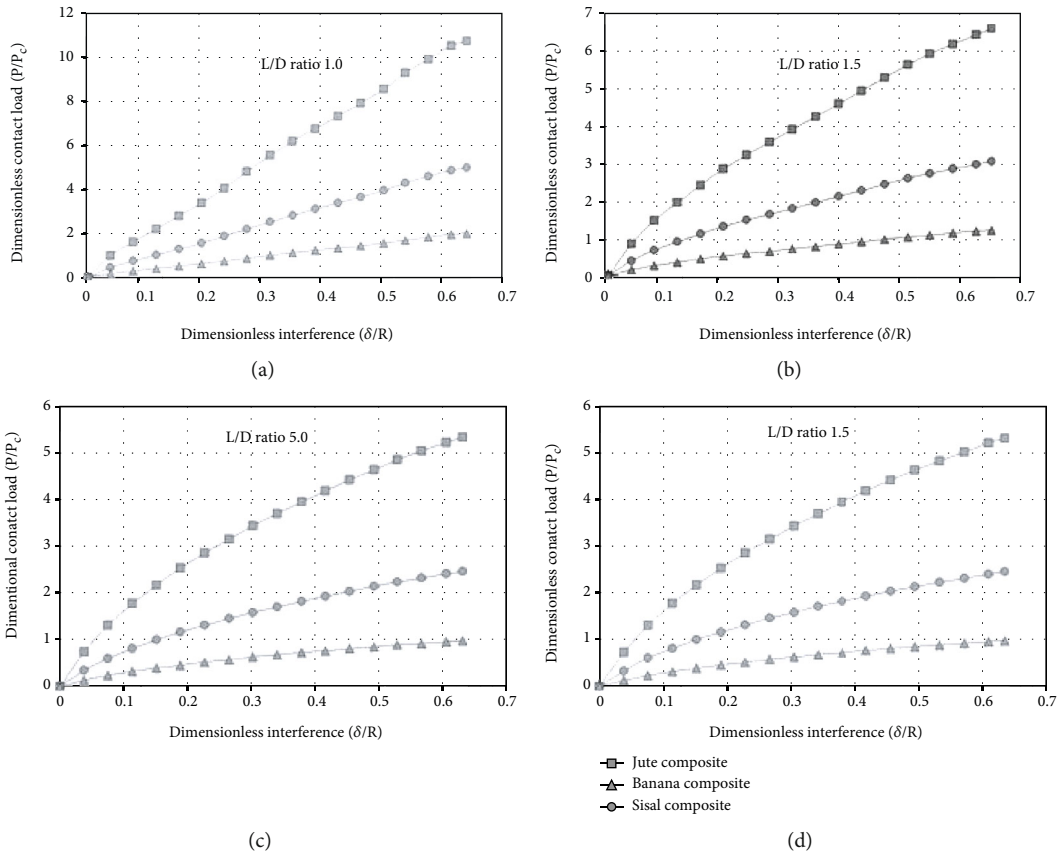

Figure 15: Response of contact load ratio vs interference ratio for various L/D ratios.

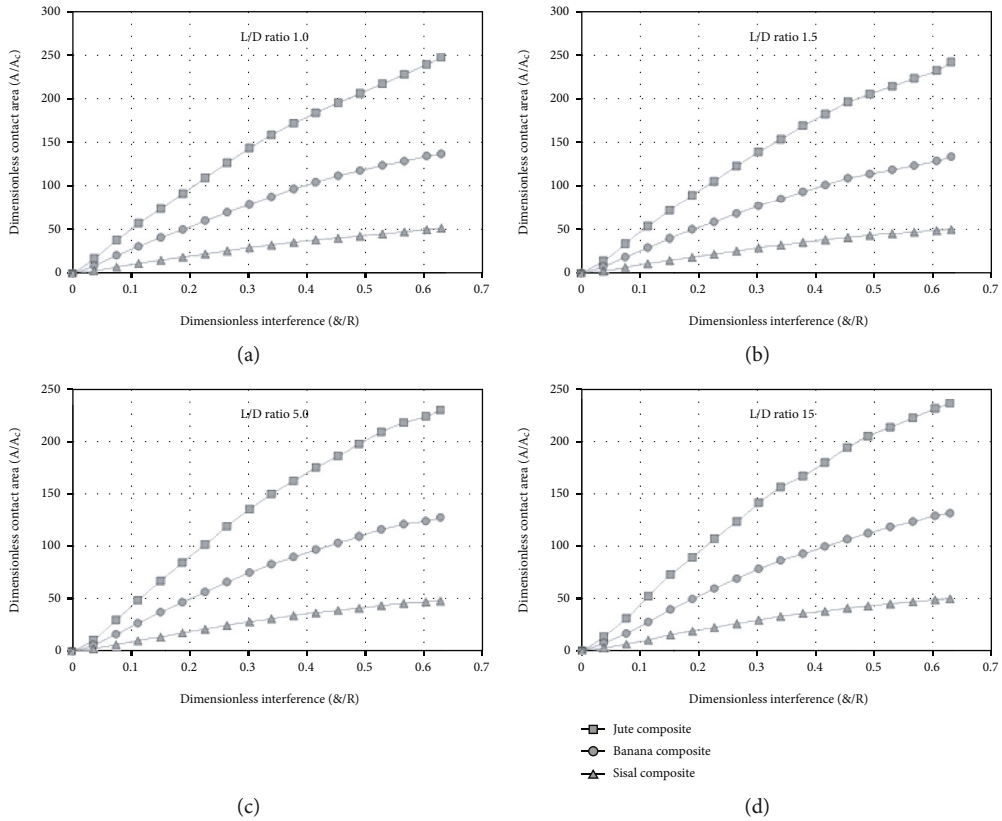

Figure 16: Response of contact area ratio vs interference ratio for various L/D ratios.

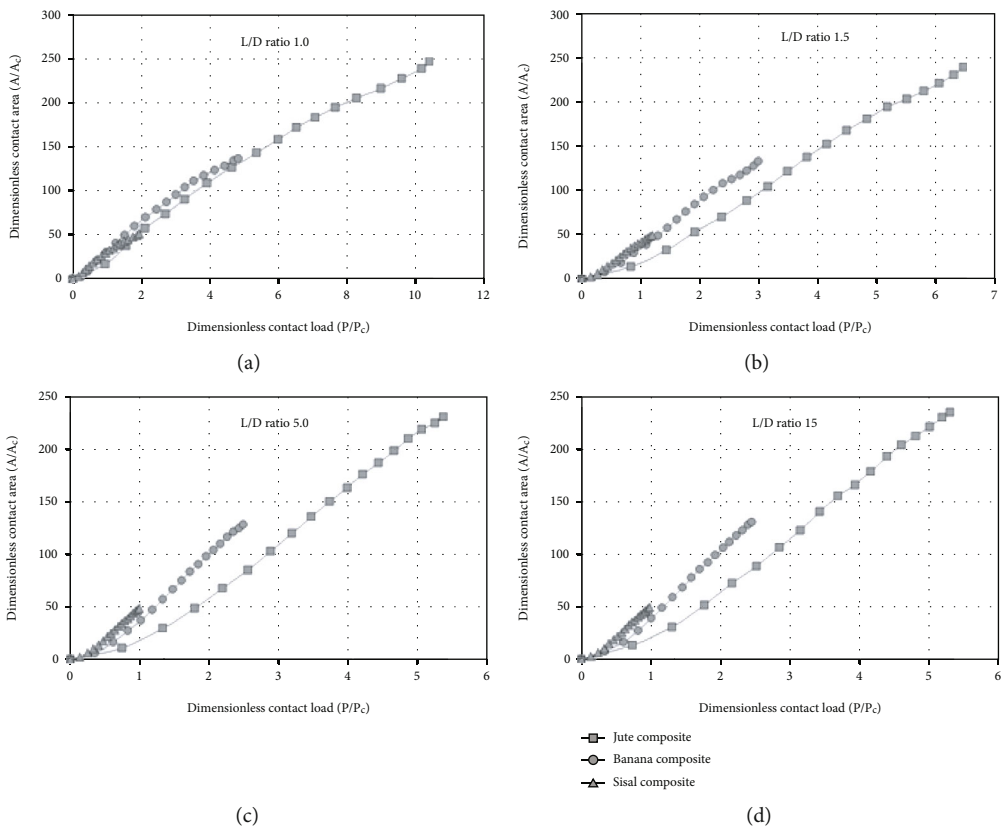

Figure 17: Response of contact area ratio vs contact load ratio for various L/D ratios.

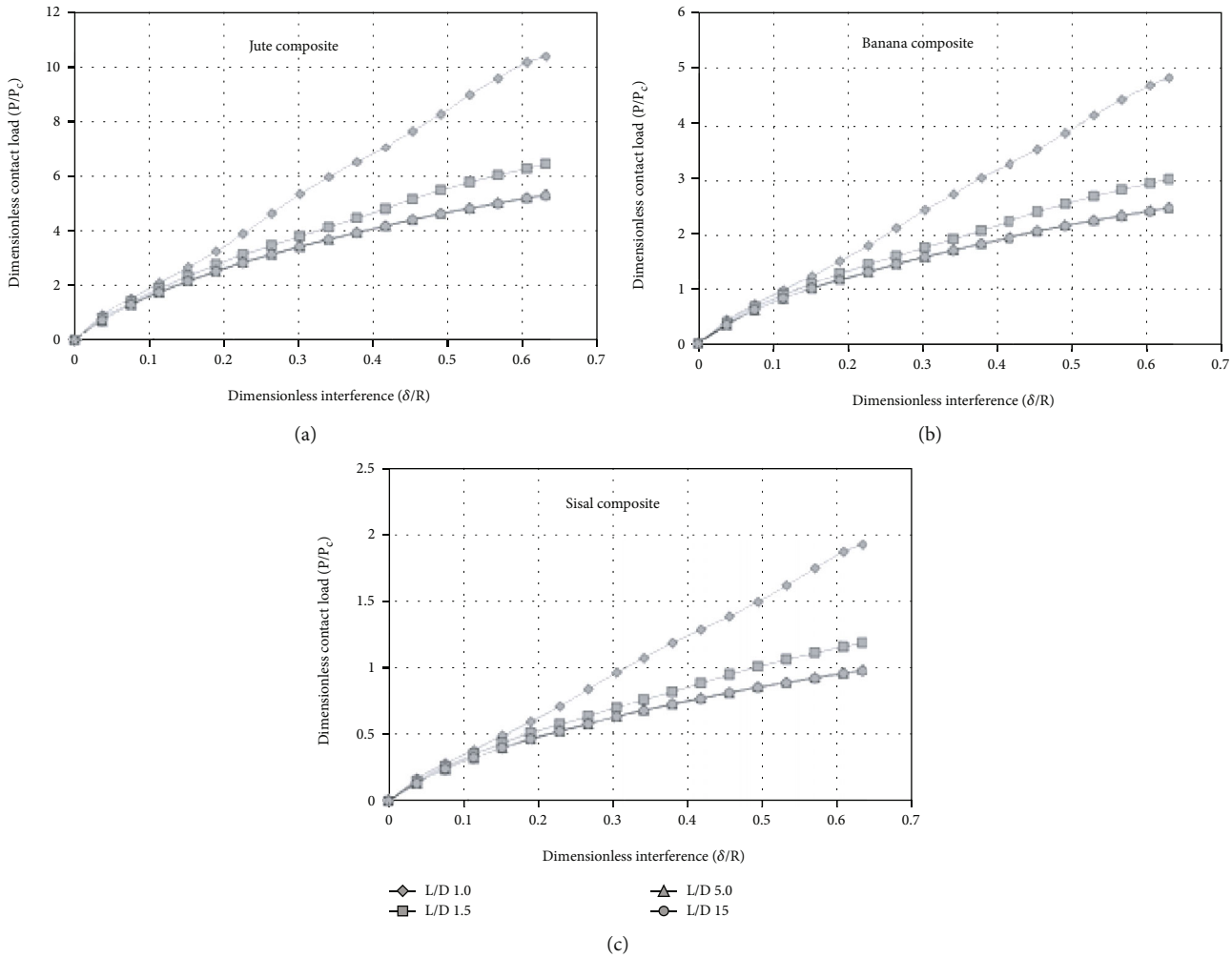

Figure 18: Response of contact load ratio vs interference ratio for various L/D ratios of composites.

3.2.1. Effect of Contact Load. The response of contact load ratio against the interference ratio for the L/D ratios of 1.0, 1.5, 5.0, and 15 is shown in Figures 15(a)–15(d).

As the interference ratio increases the contact load ratio increases for all fiber-reinforced composites. The load-bearing capacity of all the composites decreases with increase in L/D ratio. The jute fiber-reinforced composite shows high load-carrying capacity compared to all other fiber-reinforced composites. The sisal fiber-reinforced composite has low load-carrying capacity and the banana fiber-reinforced composites shows an intermediate behavior as L/D ratio increases.

3.2.2. Effect of Contact Area. From the analysis results, the contact area for every step is calculated. The response of the contact area ratio against the interference ratio for the L/D ratios of 1.0, 1.5, 5.0, and 15 is shown in Figures 16(a)–16(d). The response of the contact area ratio against the contact load ratio for various L/D ratios of 1.0, 1.5, 5.0, and 15 is shown in Figures 17(a)–17(d).

As the interference ratio increases, the contact area ratio increases nonlinearly for all fiber-reinforced composites. The jute fiber-reinforced composite shows large load-bearing area compared to all other fiber-reinforced composites. As the L/D ratio increases, the load-bearing area slightly decreases for all the composites.

3.2.3. Effect of E/Y Ratio on Contact Area against Contact Load. As the contact load ratio increases, the contact area ratio also increases linearly, but on the other hand as the L/D ratio increases, the load-bearing area also increases for increasing dimensionless load in all the composites due to the variation in E/Y ratio.

3.2.4. Effect of L/D Ratio on Contact Load against Interference. The influence of the L/D ratio on the contact load ratio against the interference ratio and dimensionless contact area shows significant difference in all the composites.

In Figure 18, the load-bearing capacity is high for jute composite, for sisal composite is low and intermediate for banana composite, but as the dimensionless interference increases, the load-bearing capacity decreases for increasing L/D ratio.

In Figures 19(a)–19(c), for the high L/D ratio, the load-bearing area is high only at low load ratio, but for high load

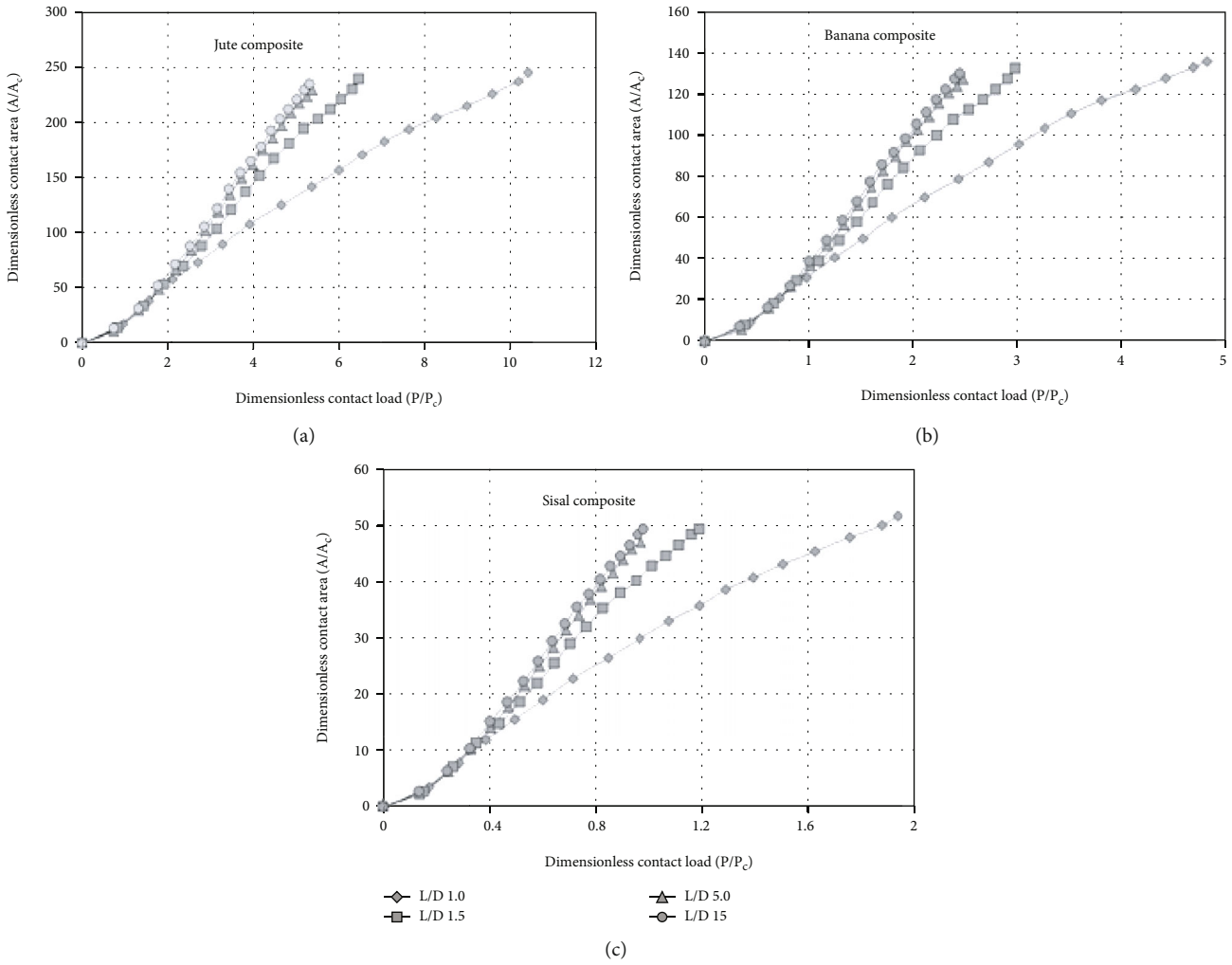

Figure 19: Response of contact area ratio against contact load ratio for various L/D ratios of composites.

ratio, the load-bearing area increases for smaller L/D ratio, and similar behaviors are observed in banana and sisal composites, but their load-bearing area and load-carrying capacity are less.

3.2.5. Effect of L/D Ratio on Von Mises Stress Distribution. The resultant Von Mises stress plots for jute-polypropylene composite at δ/R of 0.529133 for different L/D ratios are shown in Figures 20(a)–20(d). As the L/D ratio increases the maximum stress decreases.

The resultant Von Mises stress plots for banana-polypropylene composite at δ/R of 0.529133 for different L/D ratios are shown in Figures 21(a)–21(d). As the L/D ratio increases the maximum stress decreases.

The resultant Von Mises stress plots for sisal-polypropylene composite at δ/R of 0.529133 for different L/D ratios are shown in Figures 22(a)–22(d). As the L/D ratio increases, the maximum stress decreases.

Empirical relations are developed for contact parameters with variables as dimensionless interference and ratio of distance between fiber centers to diameter of fiber:

$$\begin{aligned}\frac{P}{P_c} &= -3966.91 + 3966.0027\,\frac{\delta}{R} - 303.25\left(\frac{\delta}{R}\right)^{1.5} \\ &\quad - 1767.20\left(\frac{\delta}{R}\right)^{2} - \frac{193.79\delta/R}{\operatorname{In}\delta/R} + 3956.94\left(-193.79^{-\delta/R}\right) \\ &\quad - 2.07\left(\frac{L}{D}\right) - 13.020\left(\frac{L}{D}\right)\operatorname{In}\left(\frac{L}{D}\right) + 11.366\left(\frac{L}{D}\right)^{1.5}, \\ \frac{A}{A_c} &= -412.85 + 267.56\frac{\delta}{R} + 1664.56\left(\frac{\delta}{R}\right)^{2} - 18099.34\left(\frac{\delta}{R}\right)^{3} \\ &\quad + 64608.36\left(\frac{\delta}{R}\right)^{4} - 77774.008\left(\frac{\delta}{R}\right)^{5} + 729.37\left(\frac{L}{D}\right) \\ &\quad - 478.78\left(\frac{L}{D}\right)^{2} + 138.04\left(\frac{L}{D}\right)^{3} - 14.75\left(\frac{L}{D}\right)^{4}.\end{aligned} \tag{1}$$

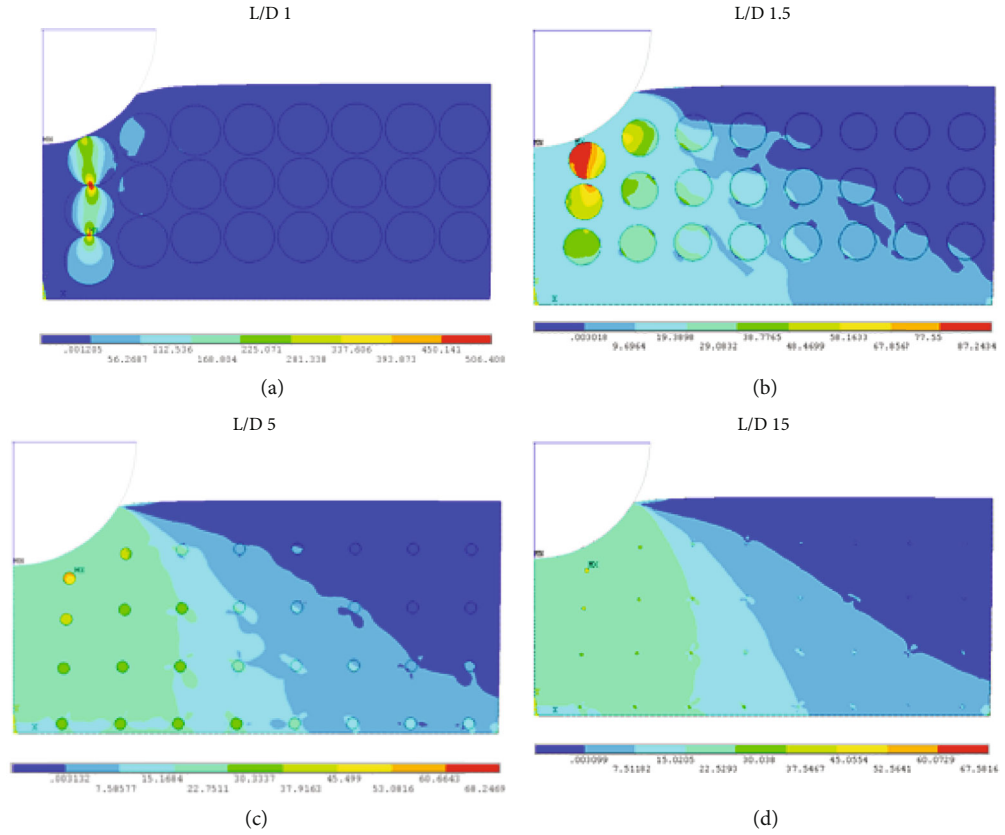

Figure 20: Von Mises stress plot for jute-polypropylene composite for various L/D ratios.

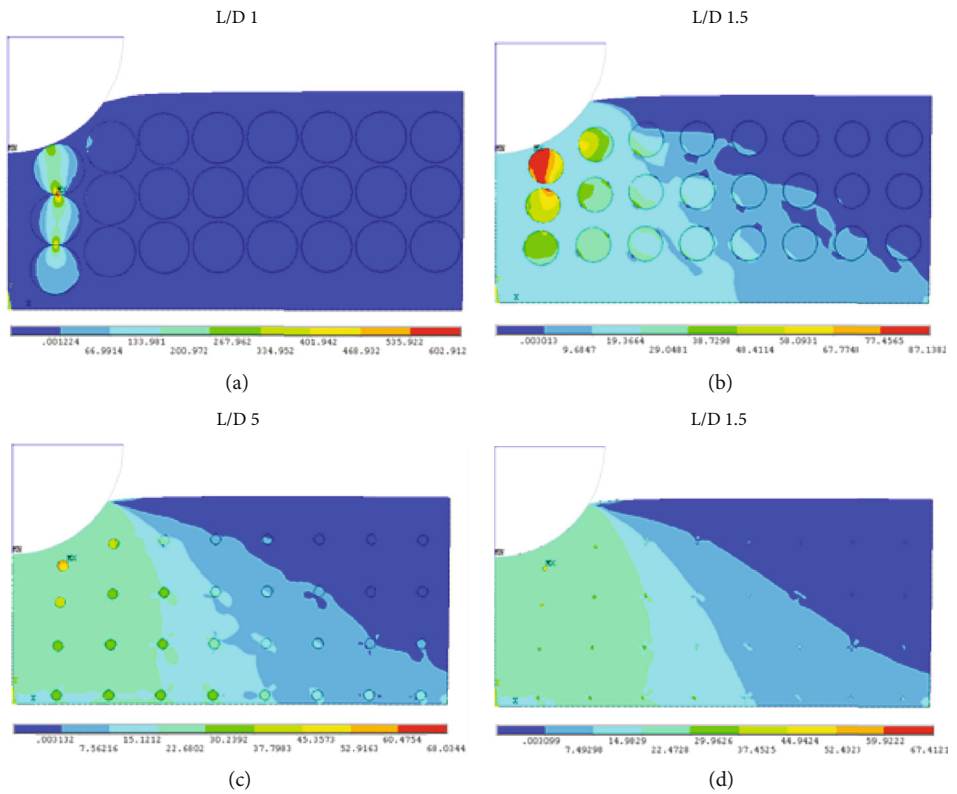

Figure 21: Von Mises stress plot for banana-polypropylene composite for various L/D ratios.

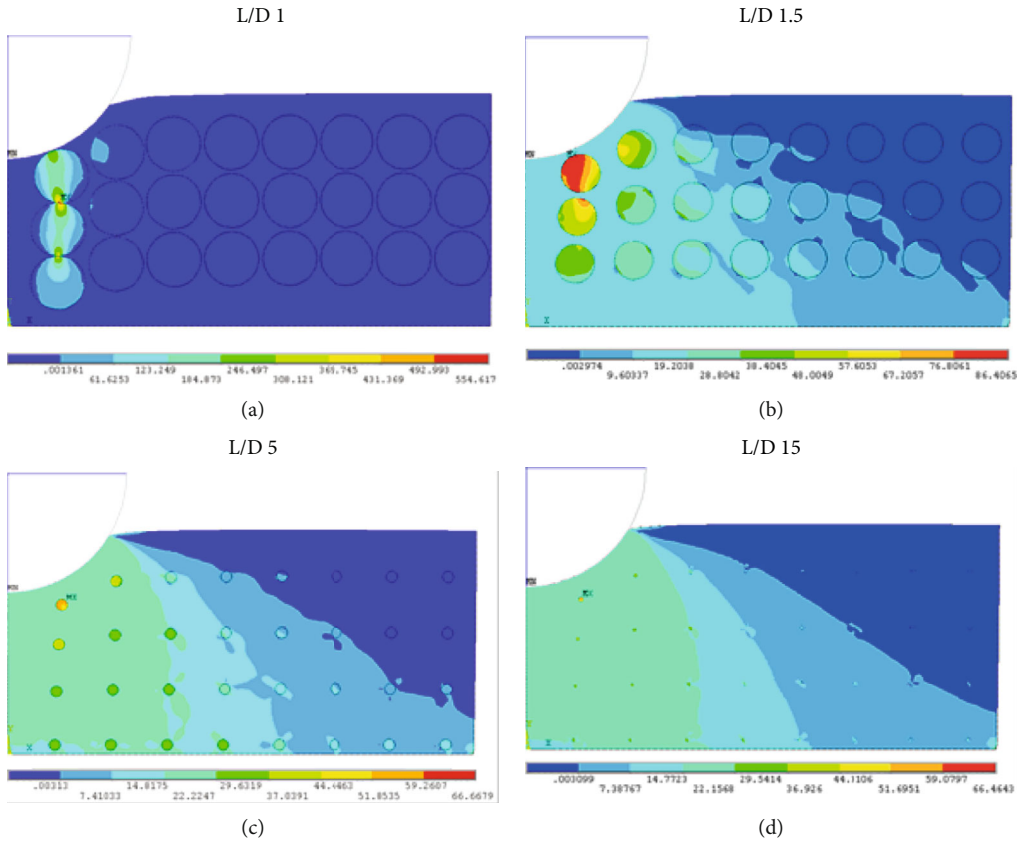

Figure 22: Von Mises stress plot for sisal-polypropylene composite for various L/D ratios.

4. Conclusion

Indentation analyses are carried on sisal-polypropylene, jute-polypropylene, and banana-polypropylene natural composites through finite element method. The results revealed that the neat polypropylene undergone three different modes of (elastic, elastoplastic, and full plastic) deformation regimes, but the indentation of the sisal-polypropylene, jute-polypropylene, and banana-polypropylene composites exposed only elastic deformation and stayed away from the elastic-plastic and plastic deformations.

As the distance between fiber centers increases, the contact load ratio increases nonlinearly for all composites. The load-carrying capacity of jute fiber composite is six times, and the bearing area ratio is five times greater than sisal fiber composite at maximum interference ratio. The impact of subsurface stress gets reduced as the distance between fiber centers increases. Compared to varying the distance between the fiber's center, the variation in diameter of fiber influences significantly. After the L/D ratio of 1.0, for the same contact load ratio, the bearing area support is double for jute-polypropylene composite compared to sisal-polypropylene composite. Compared to the sisal-polypropylene composite, for the same interference ratio, the load-carrying capacity is two times high for banana-polypropylene composite, whereas four times high for jute-polypropylene composite compared to sisal-polypropylene composite, but this effect decreases as the L/D ratio decreases. The subsurface stress gets distributed in all composites as the L/D ratio increases. In overall, the jute-polypropylene composite shows a high load-carrying capacity than other composites so this can be utilized in high load-carrying applications.

Generalized empirical relations are developed to appropriately calculate contact load, contact area with variables as interference ratio, and ratio of distance between the fiber centers and diameter of fiber.

Data Availability

The data are made available within this article.

Conflicts of Interest

The authors declare that they have no conflict of interest.

References

[1] A. Verma, A. Gaur, and V. K. Singh, "Mechanical properties and microstructure of starch and sisal fiber biocomposite modified with epoxy resin," *Materials Performance and Characterization*, vol. 6, no. 1, pp. 20170069–20170520, 2017.

[2] A. Verma, K. Joshi, A. Gaur, and V. K. Singh, "Starch-jute fiber hybrid biocomposite modified with an epoxy resin coating: fabrication and experimental characterization," *Journal of the Mechanical Behavior of Materials*, vol. 27, no. 5-6, 2018.

[3] A. Verma, C. Singh, V. K. Singh, and N. Jain, "Fabrication and characterization of chitosan-coated sisal fiber–phytagel

modified soy protein-based green composite," *Journal of Composite Materials*, vol. 53, no. 18, pp. 2481–2504, 2019.

[4] R. Vijay, D. Lenin Singaravelu, A. Vinod et al., "Characterization of raw and alkali treated new natural cellulosic fibers from _Tridax procumbens_," *International Journal of Biological Macromolecules*, vol. 125, pp. 99–108, 2019.

[5] S. Dinesh, P. Kumaran, S. Mohanamurugan et al., "Influence of wood dust fillers on the mechanical, thermal, water absorption and biodegradation characteristics of jute fiber epoxy composites," *Journal of Polymer Research*, vol. 27, no. 1, p. 9, 2020.

[6] S. Jothibasu, S. Mohanamurugan, R. Vijay, D. Lenin Singaravelu, A. Vinod, and M. R. Sanjay, "Investigation on the mechanical behavior of areca sheath fibers/jute fibers/glass fabrics reinforced hybrid composite for light weight applications," *Journal of Industrial Textiles*, vol. 49, no. 8, pp. 1036–1060, 2020.

[7] R. Vijay, A. Vinod, R. Kathiravan, S. Siengchin, and S. D. Lenin, "Evaluation of Azadirachta indica seed/spent Camellia sinensis bio-filler based jute fabrics-epoxy composites: experimental and numerical studies," *Journal of Industrial Textiles*, vol. 49, no. 9, pp. 1252–1277, 2020.

[8] R. Vijay, S. Manoharan, S. Arjun, A. Vinod, and D. Lenin Singaravelu, "Characterization of silane-treated and untreated natural fibers from stem of Leucas Aspera," *Journal of Natural Fibers*, vol. 18, no. 12, pp. 1957–1973, 2021.

[9] R. Vijay, J. D. James Dhilip, S. Gowtham et al., "Characterization of natural cellulose fiber from barks of Vachellia farnesiana," *Journal of Natural fibers*, vol. 19, no. 4, pp. 1343–1352, 2022.

[10] R. Sathish Kumar and D. M. Nivedhitha, "Mechanical characteristics study of chemically modified kenaf fiber reinforced epoxy Composites," *Journal of Natural Fibers*, vol. 19, no. 7, pp. 2457–2467, 2022.

[11] D. Tabor, *The Hardness of Metals*, Clarendon Press, Oxford, England, 1951.

[12] A. Y. Ishlinsky, "Axially symmetric problem in plasticity and Brinell's hardness test," *Journal of Applied Mathematics and Mechanics (Russian Translation is Prikladnaya Matematika i Mekhanika)*, vol. 8, pp. 201–224, 1994.

[13] R. Hill, *The Mathematical Theory of Plasticity*, Oxford University Press, London, 1967.

[14] K. L. Johnson, *Contact Mechanics*, Cambridge University Press, Cambridge, England, 2012.

[15] L. E. Samuels and T. O. Mulhearn, "An experimental investigation of the deformed zone associated with indentation hardness impressions," *Journal of the Mechanics and Physics of Solids*, vol. 5, no. 2, pp. 125–134, 1957.

[16] C. C. Hardy, C. N. Baronet, and G. V. Tordion, "The elasto-plastic indentation of a half-space by a rigid sphere," *International Journal for numerical methods in engineering*, vol. 3, no. 4, pp. 451–462, 1971.

[17] P. S. Follansbee and G. B. Sinclair, "Quasi-static normal indentation of an elasto-plastic half-space by a rigid sphere-I. Analysis," *International journal of solids and structures*, vol. 20, no. 1, pp. 81–91, 1984.

[18] A. E. Giannakopoulos, P. L. Larsson, and R. Vestergaard, "Analysis of vickers indentation," *International Journal of Solids and Structures*, vol. 31, no. 19, pp. 2679–2708, 1994.

[19] K. Komvopoulos and N. Ye, "Three-dimensional contact analysis of elastic-plastic layered media with fractal surface topographies," *Journal of Tribology*, vol. 123, no. 3, pp. 632–640, 2001.

[20] Y. J. Park and G. M. Pharr, "Nanoindentation with spherical indenters: finite element studies of deformation in the elastic-plastic transition regime," *Thin Solid Films*, vol. 447, pp. 246–250, 2004.

[21] S. D. Mesarovic and N. A. Fleck, "Spherical indentation of elastic-plastic solids," *Proceedings of the Royal Society of London. Series A: Mathematical, Physical and Engineering Sciences*, vol. A455, pp. 2707–2728, 1999.

[22] A. K. Bhattacharya and W. D. Nix, "Finite element simulation of indentation experiments," *International Journal of Solids and Structures*, vol. 24, no. 9, pp. 881–891, 1988.

[23] J. A. Knapp, D. M. Follstaedt, S. M. Myers, J. C. Barbour, and T. A. Friedmann, "Finite-element modeling of nanoindentation," *Journal of Applied Physics*, vol. 85, no. 3, pp. 1460–1474, 1999.

[24] R. L. Jackson and I. Green, "A finite element study of elasto-plastic hemispherical contact," in *Proceedings of the STLE/ASME 2003 International Joint Tribology Conference. Contact Mechanics*, pp. 65–72, Ponte Vedra Beach, Florida, USA, October 2003.

[25] W. R. Chang, I. Etsion, and D. B. Bogy, "An elastic-plastic model for the contact of rough surfaces," *The Journal of Tribology*, vol. 109, no. 2, pp. 257–263, 1987.

[26] C. Thornton, "Coefficient of restitution for collinear collisions of elastic perfectly plastic spheres," *Journal of Applied Mechanics*, vol. 64, no. 2, pp. 383–386, 1997.

[27] S. Kocharski, T. Klimczak, A. Polijaniuk, and J. Kaczmarek, "Finite-elements model for the contact of rough surfaces," *Wear*, vol. 177, no. 1, pp. 1–13, 1994.

[28] L. Vu-Quoc, X. Zhang, and L. Lesburg, "A normal force-displacement model for contacting spheres accounting for plastic deformation: force-driven formulation," *Journal of Applied Mechanics*, vol. 67, no. 2, pp. 363–371, 2000.

[29] L. Kogut and I. Etsion, "Elastic-plastic contact analysis of a sphere and a rigid flat," *Journal of Applied Mechanics*, vol. 69, no. 5, pp. 657–662, 2002.

[30] J. J. Quicksall, R. L. Jackson, and I. Green, "Elasto-plastic hemispherical contact models for various mechanical properties," *Proceedings of the Institution of Mechanical Engineers, Part J: Journal of Engineering Tribology*, vol. 218, no. 4, pp. 313–322, 2004.

[31] R. L. Jackson and I. Green, "A finite element study of elasto-plastic hemispherical contact against a rigid flat," *Journal of Tribology*, vol. 127, no. 2, pp. 343–354, 2005.

[32] V. Brizmer, Y. Kligerman, and I. Etsion, "The effect of contact conditions and material properties on the elasticity terminus of a spherical contact," *International Journal of Solids and Structures*, vol. 43, no. 18-19, pp. 5736–5749, 2006.

[33] A. Ovcharenko, G. Halperin, G. Verberne, and I. Etsion, "In situ investigation of the contact area in elastic-plastic spherical contact during loading-unloading," *Tribology Letters*, vol. 25, no. 2, pp. 153–160, 2007.

[34] R. L. Jackson and L. Kogut, "A comparison of flattening and indentation approaches for contact mechanics modeling of single asperity contacts," *Journal of Tribology*, vol. 128, no. 1, pp. 209–212, 2006.

[35] L. Kogut and K. Komvopoulos, "Analysis of the spherical indentation cycle for elastic-perfectly plastic solids," *Journal of Materials Research*, vol. 19, no. 12, pp. 3641–3653, 2004.

[36] A. Wagh, P. Maimi, N. Blanco, and D. Trias, "Predictive model for the spherical indentation of composite laminates with finite thickness," *Composite Structures*, vol. 153, pp. 468–477, 2016.

[37] L. Zhou, S. Wang, L. Li, H. Wei, and A. Dai, "An approximate solution of the spherical indentation on a generally anisotropic elastic half-space," *International Journal of Solids and Structures*, vol. 161, pp. 174–181, 2019.

[38] Y. Cao, X. Qian, and N. Huber, "Spherical indentation into elastoplastic materials: Indentation-response based definitions of the representative strain," *Materials Science and Engineering: A*, vol. 454-455, pp. 1–13, 2007.

[39] N. Venkateshwaran and A. Elayaperumal, "Banana fiber reinforced polymer composites-a review," *Journal of Reinforced Plastics and Composites*, vol. 29, no. 15, pp. 2387–2396, 2010.

[40] M. Haque, S. Islam, S. Islam, N. Islam, M. Huque, and M. Hasan, "Physicomechanical properties of chemically treated palm fiber reinforced polypropylene composites," *Journal of Reinforced Plastics and Composites*, vol. 29, no. 11, pp. 1734–1742, 2010.

[41] T. H. Quazi, A. K. Shubhra, M. M. Alam, and M. A. Quaiyyum, "Mechanical properties of polypropylene composites: a review," *Journal of Thermoplastic Composite Materials*, vol. 26, no. 3, pp. 362–391, 2013.